High-velocity-friction test for frictional properties of the rupture surface of a carbonate rock avalanche

M. Zhang, L. Yang, Z. Wang, C. Zhang, Q. Chen, and B. Wang

Faculty of Engineering, China University of Geosciences, 388#, Lumo Road, Wuhan, Hubei province 430074, People's Republic of China.

Corresponding author: Ming Zhang, email: (zhangming@cug.edu.cn)

Key Points:

- Transition from shear- and rate-strengthening to shear- and rate-weakening occurs when shear rate exceeds a critical value.
- Calcite on the limestone sample surface decomposed to CaO nanograin aggregates and CO_2 gas.
- Friction coefficient on the rupture surface reduced to less than 0.1 because of nanograin lubrication and CO_2 gas emission.

Abstract To investigate frictional properties of the rupture surface of the carbonate Jiweishan rock avalanche, we conducted high-velocity-friction tests at different shear rates. The samples showed shear- and rate-strengthening of friction at low shear rates, but transformed to shear- and rate-weakening of friction at large shear rates. The friction coefficient reduced to an extremely low value of less than 0.1. The sliding rock mass therefore could slide out of the rupture surface at a high velocity and consequently traveled a long distance as granular debris. Two mechanisms may have reduced the frictional resistance. Recrystallized calcite nanograins and CaO nanograins produced through calcite decomposition covered and lubricated the shear surface. Furthermore, the CO_2 emitted through calcite decomposition reduced the effective normal stress and therefore the friction on the surface. Our conclusions for Jiweishan rock avalanche are also useful for understanding the high mobility of other widely distributed carbonate rock avalanches.

Plain language summary

Rock avalanche, which is a kind of rock slope failure, can move several or even tens of kilometers and cause a serious loss of life and property. Frictional resistance of the failure surface on which the detached rock mass slid plays an important role in the long-distance movement of the rock mass. In order to obtain frictional resistance along the failure surface of the Jiweishan rock avalanche, we conducted high-velocity-friction tests, which can simulate long-distance shearing, on the limestone and shale rocks corresponding to the both sides of the failure surface. The

results indicated that when the shear speed exceeded a critical value, the friction decreased with increased shear rate and shear displacement. The friction coefficient can reduce to an extremely low value of less than 0.1. The limestone decomposed into CaO nanograins and CO_2 gas during shearing. The nanograins lubrication and gas emission caused low friction resistance along the shear surfaces. This is an important reason why the detached rock mass of Jiweishan rock avalanche could accelerate rapidly on the rupture surface.

1 Introduction

Frictional resistance along the rupture surface is one of the main factors controlling the velocity at which a detached rock mass can slide out of the rupture surface and therefore it affects the mobility of rock avalanches (Hungr, 2007; Zhang & Yin, 2013; Scaringi et al., 2017). Most scholars have agreed that reduction or even loss of strength along the rupture surface leads to the rapid initiation and sliding of a displaced rock mass (Hungr, 2007; Leroueil, 2001; Wang et al., 2010; Lucas et al., 2014; Alonso et al., 2016; Song et al., 2016) before it moves out of the toe of the rupture surface (Zhang et al., 2016). However, the mechanisms causing the strength decrease are very complicated and much debated.

To determine frictional resistance variations in shear zone soils, ring shear apparatus, which can mimick localized and intense shear behavior, have been used to investigate various factors and mechanisms (Sassa, 1985; Tika et al., 1996; Sassa et al., 2004, 2005; Wang et al., 2010; Zhang et al., 2011; Miao et al., 2014; Scaringi &

Di Miao, 2016; Scaringi et al., 2017; Wu et al., 2017, 2019). Three effects of shear rate on the residual strength have been observed: positive (rate-strengthening), neutral (rate-unchanging) and negative effect (rate-weakening) (Tika et al., 1996; Leroueil, 2001). Shearing mode transition (Lupini et al., 1981; Saito et al., 2006; Wang et al., 2010), grain breakage and layering (Wang & Sassa, 2000; Agung et al., 2004; Zhang et al., 2011), pore water pressure (Tika et al., 1996), and mineral alignment (Wang et al., 2010) have been proposed to interpret the friction variation.

Due to the shortcomings of traditional rock mechanic tests, frictional resistance along the rupture surface in rock avalanches remains largely unexplored, although analyses and observations suggest a low mobilized friction coefficient during their runout (Lucas et al., 2014; Alonso et al., 2016; Scaringi et al., 2017). Several hypotheses have been proposed, such as frictional heating (Voight & Faust, 1982; Hendron & Patton, 1985), frictional-heat-triggered gaseous pore pressure (Habib, 1975; Goren & Aharonov, 2007; Goren et al., 2010), and frictional-heat-triggered mineral decomposition and production of CO_2 (Erismann, 1979; Erismann & Abele, 2001), but none has been experimentally proven or ruled out.

In recent years, high-velocity-friction tests originally designed to examine the frictional properties of seismic fault planes (Shimamoto & Tsutsumi, 1994; Yao et al., 2016), have been used to test frictional resistance variation during the sliding of detached rock masses on the rupture surface of rock avalanches. Yang et al. (2014) conducted high-velocity-friction tests on gouge from faults parallel to the bedding under semi-wet conditions at a normal stress corresponding to the overburden pressure of the landslide mass. They found that slip-weakening was essential in initiating the landslide and a low friction coefficient (0.08-0.1) made the high speed of the landslide possible. Hu et al. (2018) used high-velocity-friction tests to replicate the temperatures and mineral changes on the rupture surface during initiation. They confirmed heating above 800 °C on the rupture surface, and thermal decomposition of dolomite to magnesium and calcium oxides in the shallowest samples. These studies illustrate that high-velocity-friction tests are effective for experimentally examining the laws and mechanisms of friction resistance variation of large rock landslides.

The catastrophic Jiweishan rock avalanche had a 720-m-long rupture surface, which developed along an upper limestone and lower interbedded shale. The friction on the rupture surface was important for acceleration of the sliding rock mass during initiation and its subsequent rapid and long-distance transport. We conducted high-velocity-friction tests with limestone and shale samples from the Jiweishan rock avalanche to examine the frictional properties along the rupture surface and investigate the mechanisms by which the friction changed.

2 Case study

The Jiweishan rock avalanche occurred on 5 June 2009, and is located in Tiekuang Town, Wulong County, Chongqing, China. For the location map, see Zhang et al. (2018). The rock avalanche initially started as a rockslide and then turned into a catastrophic debris avalanche, travelling more than 1500 m and burying 74 people (Xu et al., 2010; Yin et al., 2011).

2.1 Geologic setting and characteristics of the Jiweishan rock avalanche

Since the Jiweishan rock avalanche is well documented (Yin et al., 2011; Zhang & McSaveney, 2018), its geological setting and characteristics are just briefly described here. The source area is situated at the crest of Jiweishan Mountain, which extends roughly in a N—S direction and was deeply incised (Figure 1), with an east-facing nearly vertical cliff adjacent to Tiejiang Creek at the cliff toe (Zhang et al., 2018). The original cliff surface ranged between about 50 and 150 m high. The source area of the rock avalanche mainly consists of the Lower Permian Maokou Formation limestone, with a thickness of about 50 m, and the Lower Permian Qixia Formation limestone with a thickness of about 150 m and interbedded with thin layers of weaker shale about 10 to 30 cm thick. The rupture took place along a surface developed in the Qixia Formation along the contact between limestone and a 30-cm-thick underlying interbedded shale.

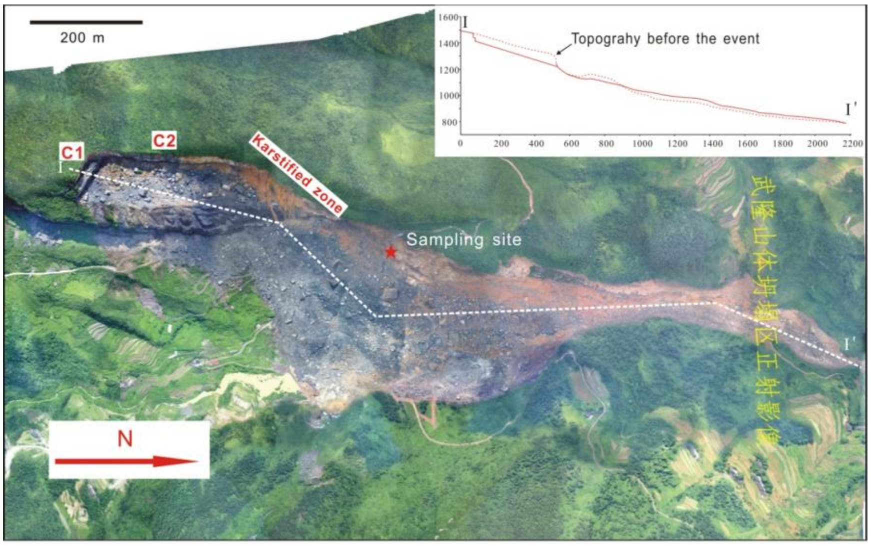

Figure 1. Remote sensing image of the Jiweishan rock avalanche. The yellow Chinese characters mean “Orthographic image of the Jiweishan rock avalanche”.

The boundary of the detached rock mass was defined by cracks C1 and C2, a karstified zone and the cliff surface (Figure 1). The detached rock mass was about 720 m long, and its maximum width was about 152 m and average thickness about 60 m. The volume was about 5×10^6 m^3 (Yin et al., 2011).

Before failure, the rock slope had gone through over 60 years of creep deformation. Cracks C1 and C2 had opened and less than 40% of the area of the karstified zone remained intact (Yin et al. 2011). The rock mass suddenly failed due to the brittle failure of the bridges in the karstified zone (Zhang & McSaveney, 2018), and then slid on the 720-m-long rupture surface, and finally slid out, landing on the ground about 50 m below the toe of the rupture surface. The sliding rock mass was transformed into granular debris as it struck the ground, and travelled about 1500 m along Tiejiang Creek (Zhang et al., 2018). In this study we investigate the frictional properties along the 720-m-long rupture surface that the rock mass slid on.

2.2 Methods and materials

We conducted high-velocity-friction tests to simulate shearing between the sliding limestone rock mass and the shale bedrock. The tests were conducted on high-velocity-friction apparatus at the Institute of Geology, China Earthquake Administration, Beijing. The apparatus was a Shimamoto III model imported from Japan in 2010. It is mainly used to investigate the physical, chemical and mechanical properties of the gouge and surfaces of fault planes.

For fault tests, rock samples corresponding to the two plates of the fault are locked at the upper rotary piston and the lower stationary piston. The samples can be a pair of solid cylinders or hollow annular cylinders with smooth surfaces. In case the rock samples fracture during shearing, they are encircled and protected by an aluminum ring. The lower sample remains stationary and the upper one revolves at a controlled constant or changing rate during shearing.

The maximum normal load of the apparatus is 8 MPa and the maximum angular velocity is 1500 rounds per minute. Because shear velocity is not constant along the radius of the cylinder, an equivalent shear rate (V_{eq}) is defined such that $V_{eq}S$ gives the rate of frictional work over a shearing surface with an area S, assuming a uniform shear stress (Shimamoto & Tsutsumi, 1994; Yang et al., 2014). For hollow annular cylinder samples with outer and inner diameters r_1 and r_2, respectively, V_{eq} is given by:

$$V_{eq} = \frac{4\pi R(r_1^2+r_1r_2+r_2^2)}{3(r_1+r_2)} \quad (1)$$

where R is the angular velocity. We used solid cylinder samples with r_1=40 mm and r_2 = 0 mm. Therefore, the maximum angular velocity gives a maximum shearing rate of 2.1 m/s. For a detailed description of the machine, see Ma et al. (2014).

Limestone and shale samples from the Jiweishan horizons identical with the source area were taken down-dip (Figure 1) and tested using X-ray diffraction (XRD) and X-ray fluorescence (XRF). The results indicated that the limestone sample was almost all calcite, while the shale sample was mainly composed of calcite, talc and quartz.

The limestone and shale samples were cut to be cylinders with a diameter of about 40 mm and a height larger than 32 mm and then sanded to be 40 mm ±40 um to ensure the upper and lower samples would contact each other closely and evenly. The samples were encircled and protected by an aluminum ring to avoid fracture during shear. To measure the temperature on the shear surface, two thermal probes were embedded through two small holes symmetrically drilled from the flank to the shear surface of the cylinder limestone samples. To prevent damage during shearing, the two probes did not reach the shear surface but ended a little bit away from the surface.

In total five tests were carried out, using five different shear rates of 0.05, 0.2, 0.5, 1.0 and 2.1 m/s. The normal load was uniformly 1.42 MPa, which corresponded to the overburden load of the sliding rock mass. All the samples had a natural moisture content, since there was no rainfall before the Jiweishan rock avalanche, and the water table was below the rupture surface (Zhang & McSaveney, 2018). The shear displacement was not determined in advance, the test was stopped when the friction coefficient tended to be roughly constant. Temperature and shear stress were monitored during shear. XRD and XRF were used to determine mineral components of the samples before and after shear. Scanning electron microscope (SEM) tests were conducted on the surfaces of the sheared limestone samples to examine changes in texture.

3 Test results

3.1 Friction coefficient and temperature curves

Figure 2 presents temperature and friction coefficient curves for the tests at shear rates of 0.05, 0.2, 0.5, 1.0 and 2.1 m/s, respectively. The friction coefficient at five different rates all increased rapidly to a peak value of 0.55 to 0.8 immediately after shearing began, then fluctuated sharply due to the rough undulating shear surfaces of the limestone and shale samples. The length of the fluctuation differed because of the roughness of the shear surfaces. For example, the curve for a shear rate of 0.5 m/s fluctuated during shear displacement from 0 to about 20 m, while the curve at a shear rate of 2.1 m/s only fluctuated during shear displacement from 0 to about 7 m.

After the fluctuation, the friction coefficient transiently decreased to a comparatively steady value, which was then followed by a gradual increase or decrease to the residual values, which differed at different shear rates. The friction coefficient at a shear rate of 0.05 m/s increased from about 0.4 to about 0.7 with increased shear displacement, showing a shear-strengthening behavior, while the friction coefficient at shear rates of 0.2, 0.5, 1.0 and 2.1 m/s decreased with increased displacement, showing a shear-weakening behavior. Notably, the friction coefficient at a shear rate of 2.1 m/s decreased from about 0.4 to less than 0.1, showing an extremely low friction.

The residual friction coefficients of the tests at shear rates of 0.05, 0.2, 0.5, 1.0 and 2.1 m/s are 0.50 to 0.70, 0.30 to 0.38, 0.27 to 0.33, 0.16 to 0.26 and 0.06 to 0.15, respectively (Figure 2f). The residual friction coefficient decreased with increased shear rate, showing a rate-weakening behavior.

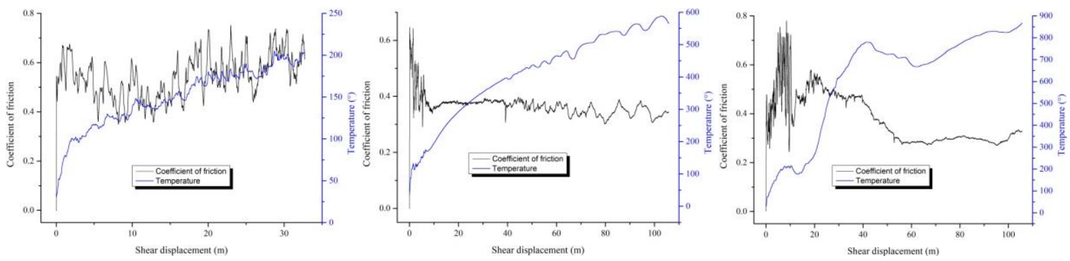

(a) V=0.05 m/s (b) V=0.2 m/s (c) V=0.5 m/s

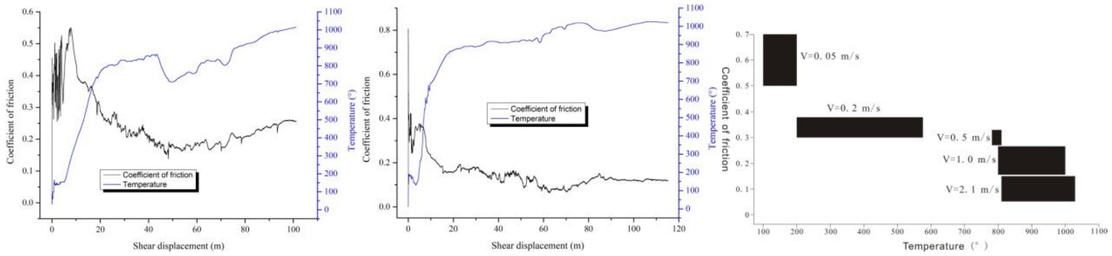

(d) V=1.0 m/s (e) V=2.1 m/s (f) Final ranges of temperature and friction coefficient

Figure 2. (a) to (e) are friction coefficient and temperature curves for different shear rates, and (f) shows the final ranges of temperature and friction coefficient at different shear rates.

The temperature on the shear surface at different shear rates increased significantly immediately after shearing began, then reached a comparatively steady value, which is called an inflection point in this study. The temperature then fluctuated more slowly, increasing or decreasing with increased shear displacement. The temperature curves at shear rates of 0.05 m and 0.2 m had subtle inflection points at about 100° and 175°, respectively, and their temperatures finally increased to about 200° and 590°, respectively. The temperature curves at shear rates of 0.5, 1.0 and 2.1 m/s had obvious inflection points at 780°, 800°and 860°, and finally increased to 810°, 1000° and 1030°, respectively. In general, the ultimate temperature increased with increased shear rate.

3.2 Components and textures on the shear surface

Figure 3 displays the samples after shear and SEM images of the shear surface of the limestone samples. Figure 3(a) shows that grey powder covered the shear surfaces of the samples at the shear rate of 0.05 m/s. XRD test result indicates that the powder was mostly the ingredients of the shale sample. It means that the weaker shale surface was abraded to powder during shear. Figure 3(b) shows that both surfaces of the samples after shear at a rate of 0.2 m/s were slickened and polished, and covered by sporadic white spots. Figures 3(c) to (e) showed that both shear surfaces of the samples after shear at rates of 0.5 to 2.1 m/s also showed slickensides and were polished, but were covered by a layer of white powder. The area and thickness of this white layer increased with increased shear rate. XRD test results indicated the white powder was CaO. We took samples outside the white powder areas of the limestone and shale sample surfaces after shear at 2.1 m/s to conduct XRD tests. The results indicated that surface outside the white powder area of the limestone sample was still mainly calcite. The surface outside the white powder area of the shale sample was mainly calcite, quartz and talc, and some newly formed minerals including magnesium silicate and enstatite.

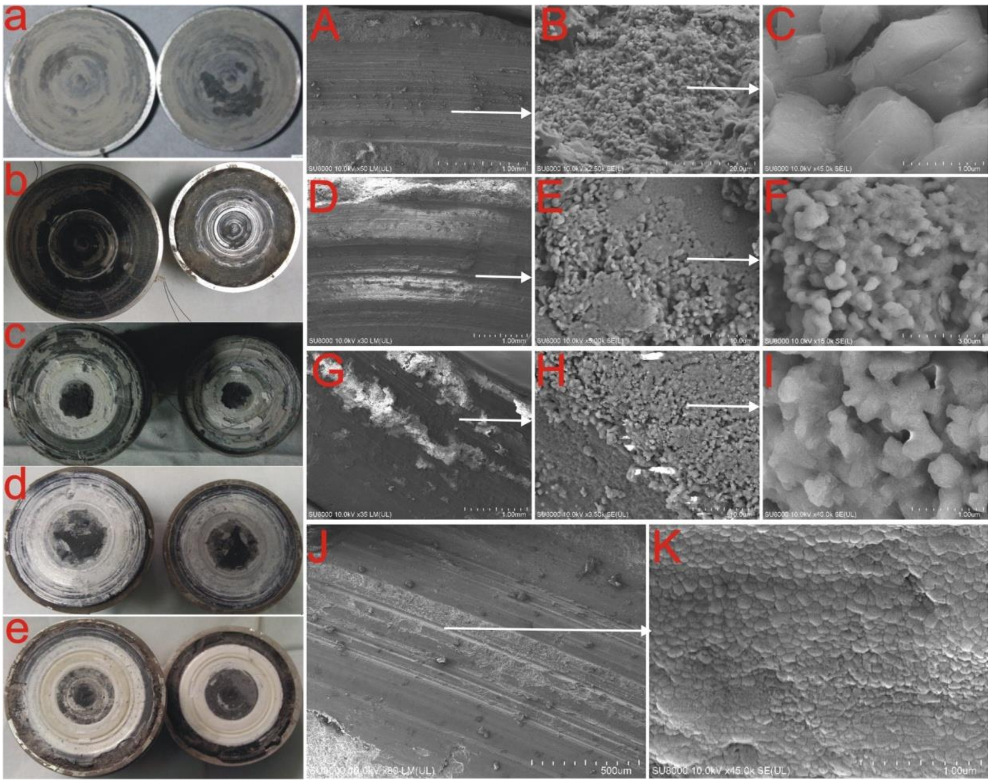

Figure 3. Samples after shear. a, b, c, d and e present the shear surfaces of the five samples after shear at different shear rates of 0.05, 0.2, 0.5, 1.0 and 2.1 m/s. A, B and C are scanning electron microscope (SEM) images at different scales of the shear

surface for a shear rate of 0.2 m/s; E, F, G are SEM images of the shear surface at a shear rate of 0.5 m/s; H, I, J at a shear rate of 1.0 m/s; and K, L at a shear rate of 2.1 m/s.

SEM tests on the black area outside the white powder covered area of the limestone surfaces at shear rates of 0.2 to 2.1 m/s were conducted to examine their texture (Figures 3(A) to (K)). The surfaces of the limestone samples were smooth, shiny and show grooves oriented parallel to the shear direction. Higher magnification images reveal that the shear surfaces consisted of recrystallized grains, and grain size decreased with increased shear rate. Figures 3(A) to (C) indicate that grains on the shear surface for a rate of 0.2 m/s were mostly about 1 um in diameter and angular in shape. Figures 3(D) to (I) indicate that particles on the shear surface for rates of 0.5 and 1 m/s were mostly between 200 and 800 nm in diameter. They were loosely arranged and roughly round in shape. Figures 3 (J) and (K) indicate that grains on the shear surface at the shear rate of 2.1 m/s were less than 200 nm in size. They were round in shape and densely arranged with straight boundaries between each other.

4 Discussion

4.1 Component and texture changes on the surface

The shear surfaces of the samples obviously had gone through mineral decomposition and recrystallization during shearing that caused mineral and texture changes. Many studies have shown that calcite decomposes to CaO and lime CO_2 gas at 600—850 °C (L’vov, 2002; Singh et al., 2002). In our tests, the temperature at the shear surface during shearing finally increased to higher than 600 °C in the tests at shear rates of 0.5, 1.0 and 2.1 m/s. Because the thermal probes did not touch the shear surface, and the temperature obtained by them was actually a little lower than the real temperature, we therefore deduce that real temperature on the shear surface of the test at rate of 0.2 m/s finally reached 600 °C or higher. Therefore, calcite on the surfaces sheared at rates of 0.2, 0.5, 1.0 and 2.1 m/s decomposed into white CaO powder and CO_2 gas, as shown in equation (1):

$$CaCO_3 \rightarrow CaO + CO_2 \quad (1)$$

Calcite on the surfaces sheared at rate of 0.05 m/s did not go through any significant chemical reaction, but mainly mechanical abrasion. In addition, because the temperature increased with increased shear rate (Figure 2f), the area and thickness of CaO powder increased with increased shear rate.

Based on the newly formed minerals, we deduce that talc in the shale sample had decomposed to anhydrous magnesium silicate and enstatite, which occurred at 630—850 °C, as shown in equations (2) and (3) (Hu et al., 2018).

$$2Mg_3Si_4(OH)_2 \rightarrow 2Mg_3Si_4O_{11} \text{ (anhydrous magnesium silicate)} + 2H_2O \text{ (gas)} \quad (2)$$

$$2Mg_3Si_4O_{11} \rightarrow 3Mg_2(Si_2O_6) \text{ (enstatite)} \quad (3)$$

Although we only tested the sample after a shear at rate 2.1 m/s to determine the component changes of the shale sample, we deduce that the reactions also occurred in the tests at rates of 0.5, 1.0 and 2.1 m/s, because their temperature all exceeded 630 °C.

As well as the aggregates of CaO nanograins (Han et al., 2010) generated, the calcite on the limestone surface also recrystallized to nanograins during shear at rates larger than 0.5 m/s (Figure 3). As a result, most of the area on the limestone surface was covered by nanograins. Furthermore, the nanograins of CaO increased in area and thickness with increased shear rate, and nanograins of recrystallized calcite outside the CaO area became denser, rounder and finer with increased shear rate.

4.2 Mechanisms of shear- and rate- weakening of friction

The friction coefficient at shear rates of 0.05 m/s and 0.2 to 2.1 m/s displayed different shearing behaviors. At 0.05 m/s, the friction coefficient increased with increased shear displacement and showed a shear-strengthening behavior, while at 0.2 to 2.1 m/s the friction coefficient decreased with increased shear displacement and shear rate, showing shear-weakening and rate-weakening behaviors. Scaring et al. (2017) conducted rotary shear tests on limestone samples from the Daguangbao mega landslide and calcareous shale samples from the Jiweishan landslide separately, under normal loads between 150 kPa and 1500 kPa, at shear rates of less than 120 mm/s, which are much lower than that of real rapid landslides, and lower than the shear rates used in this study. The results indicated that the friction coefficient increased with increased shear rate (rate-strengthening) and also with increased shear displacement (shear-strengthening). Combined with our test results, it was very likely that the friction coefficient at lower shear rate showed shear- and rate-strengthening behaviors; while at higher rate it showed shear- and rate-weakening behaviors.

Different mechanisms caused the differing shear behaviors between low- and high-rate shearing. The mechanisms responsible for shear- and rate-strengthening at low-rate shear are much debated (Kilgore et al., 1993). Marone et al. (1990) proposed that rate-strengthening was due to rate-dependent dilatancy of the gouge, and the magnitude of rate-strengthening they observed in tests varied directly with the thickness of the gouge layer. Blanpied et al. (1989) and Segall et al. (2010) suggested frictional heating can cause a transition to rate-strengthening. Biegel et al. (1992) proposed that after a roughness-dependent stiffness stage, samples reached a yield point which marked a start of the slip-hardening stage during which the shear strength of the surfaces continued to increase at a rate that depends on roughness and normal load. Rougher surfaces exhibited higher rates of slip hardening than smooth, and over much greater slip distances. In our test at a shear rate of 0.05 m/s, the shear surface went through mainly mechanical abrasion, which produced a thin layer of fine gouge (Figure 3a). The gouge dilated due to the heat produced during shear, and consequently increased friction on the shear surface. The amount of the heat increased with increased shear displacement and shear rate, therefore, the dilatancy and friction increased with increased shear displacement and shear rate, i.e. shear- and rate-strengthening behaviors. However, the heat, which mainly depended on shear rate, was not large enough to cause mineral decomposition of the limestone and calcareous shale when the shear rate was less than a critical value, which was deduced to be between 0.05 and 0.2 m/s in our tests.

When the shear rate was larger than the critical value, the friction decreased with increased shear rate and shear displacement, showing shear- and rate weakening behaviors. They were obviously related to the heating and mineral decomposition during shear.

Two mechanisms, which were proposed to explain the weakening of seismic faults, are considered to have reduced friction in our tests. The first one is nanograin lubrication (Han et al., 2010, 2011; Yao et al., 2016). As the nanopowder-coated shear surface becomes very smooth with shear displacement, fine, rounded and densely-arranged nanograins led to very low friction compared to surfaces coated in larger, looser and angular grains. The nanograins even began to roll rather than slide on the smooth surface during shear (Han et al., 2011), causing even lower friction. The second one was that CO_2 emission reduced the effective normal stress, and therefore reduced the friction on the shear surface. Han et al. (2010) conducted rotary frictional tests with carbonate rocks, and they found that calcite began to decompose and emit CO_2 if the shear rate was larger than a critical value, and the friction coefficient drop was apparently concurrent with CO_2 emission. In our tests, we did not monitor and detect emission of CO_2, but it did occur and was very likely to have reduced the friction.

Our tests indicated that temperature during shear increased with increased shear displacement and shear rate (Figure 2), and consequently more calcite decomposed into CaO nanograins and CO_2 (Figure 3). In addition, recrystallized calcite grains outside the CaO powder area on the sample surface also became finer, denser and rounder with increased temperature (Figure 3). Therefore, the samples showed shear- and rate-weakening of friction.

4.3 Mechanisms of rapid initiation of the Jiweishan rock avalanche

Observations and analyses support shear-weakening and rate-weakening mechanisms to explain the catastrophic failure and consequent hypermobility of rock avalanches (Lucas et al., 2014; Alonso et al., 2016; Scaringi et al., 2017). However, based on our test results, it is reasonable to deduce that a sliding rock mass firstly goes through shear-strengthening after initiation when its velocity is less than a critical value, and then through shear-weakening after its velocity exceeds the critical value. Finally, the friction coefficient on the rupture surface achieves a residual value. Therefore, shear displacement is needed for a sliding rock mass to achieve a critical velocity and friction coefficient on the rupture surface to reach the residual value. Handwerger et al. (2016) proposed that the transition from shear-strengthening to shear-weakening motion of a sliding rock mass requires that the length of the rupture surface exceed a critical nucleation length that is shorter for higher effective stresses. Han et al. (2010) concluded that the slip-weakening distance, this was the distance over which peak shear resistance dropped to a residual value, varied from 4 to 28 m, and became shorter at higher normal stress. In our tests, The friction coefficient at a rate of 2.1 m/s reached its residual value of less than 0.1 at a shear displacement of about 70 m (Figure 2).

In the Jiweishan rock avalanche, brittle failure of limestone rock bridges in the front karst zone (Figure 1) caused rapid initiation and acceleration of the sliding rock mass (Zhang & McSaveney, 2018). Therefore, it is reasonable to deduce that the speed of the sliding rock mass could accelerate to 2.1 m/s quickly, and that the friction coefficient at the rupture surface of the Jiweishan rock avalanche decreased to an extremely low value of less than 0.1 after a shear displacement about 70 m. Most of the 700-m-long sliding rock mass of the Jiweishan rock avalanche thus slid and accelerated on a rupture surface with an extremely low friction, and then could slide out at a high speed. This was a major contribution to the rapid and long-runout transport of the Jiweishan rock avalanche.

5 Conclusions

High velocity friction tests were used to investigate the frictional properties along the rupture surface of the Jiweishan rock avalanche. The results indicated that shear-strengthening and rate-strengthening of friction occurred on the rupture surface when the sliding rock mass slid at a low velocity less than a critical value, probably due to the thermal expansion of abrasion-induced gouge. Shear-weakening and rate-weakening of friction occurred when the sliding rock mass slid at a high velocity larger than the critical value. Two mechanisms may have contributed to the shear behaviors on the rupture surface of rock avalanche. The calcite on the limestone sample surface decomposed to CaO nanograin aggregates and CO_2 gas. The calcite minerals that did not decompose on the surface also recrystallized into nanograins. Nanograin lubrication and a CO_2-induced decrease of effective normal stress produced extremely low friction on the rupture surface. The sliding rock mass therefore could slide out of the rupture surface at a high speed, and was then followed by rapid and long-runout transport.

This paper has investigated the frictional properties on the rupture surface of the carbonate Jiweishan rock avalanche. But our conclusions are also applicable for explaining the high mobility of other widely distributed rock avalanches in carbonate rocks.

Acknowledgements This work was supported by the National Natural Science Foundation of China (41472264, 41772334, and 41920104007) and the Fundamental Research Founds for National University, China University of Geosciences (Wuhan) (CUGCJ1802). We thank Dr. Eileen McSaveney for editing our paper to make it more readable. All data are publicly available online (https://pan.baidu.com/s/4srnQGI5).

References

Agung, M.W., K. Sassa, H. Fukuoka, and G. Wang (2004), Evolution of shear zone structure in undrained ring-shear tests, Landslides, 1(2): 101-112.

Alonso, E.E., A. Zervos, and N.M. Pinyol (2016), Thermo-poro-mechanical analysis of landslides: from creeping behavior to catastrophic failure, Geotechnique, 66(3): 202-219.

Biegel, R.L., W. Wang, C.H. Scholz, G.N. Boitnott, and N. Yoshioka (1992), Micromechanics of rock friction 1. Effect of surface roughness on initial friction and slip hardening in westerly granite, Journal of Geophysical Research, 97: 8951-8964.

Blanpied, M.L., T.E. Tullis, and J.D. Weeks (1998), Effects of slip, slip rate, and shear heating on the friction of granite, Journal of Geophysical Research, 103: 489-511.

Erismann, T.H. (1979), Mechanisms of large landslides, Rock Mechanics, 12: 15- 46.

Erismann, T.H., and G. Abele (2001), Dynamics of rockslides and rockfalls. Springer-Verlag, Berlin Heidelberg, New York, 2001, 316 pp.

Goren, L., and E. Aharonov (2007), Long runout landslides: The role of frictional heating and hydraulic diffusivity, Geophysical research letters, 34(L07301): 1-7.

Goren, L., E. Aharonov, and M.H. Anders (2010), The long runout of the mountain landslide: Heating, pressurization, and carbonate decomposition, Journal of Geophysical Research, 2010, 115(B10210): 1-15.

Habib, P. (1975), Production of gaseous pore pressure during rockslide, Rock Mechanics, 7(4): 193-197.

Han, R., T. Hirose, and T. Shimamoto (2010), Strong velocity weakening and powder lubrication of simulated carbonate faults at seismic slip rates, Journal of Geophysical Research, 115: B03412.

Han, R., T. Hirose, T. Shimamoto, Y. Lee, and J. Ando (2011), Granular nanoparticles lubricate faults during seismic slip, Geology, 39: 599-602.

Handwerger, A.L., A.W. Rempel, R.M. Skarbek, J.J. Roering, and G.E. Hillery (2016), Rate-weakening friction characterizes both slow sliding and catastrophic failure of landslides, Proceedings of the National Academy of Sciences of the United States of America, 113(37): 10281-10286.

Hendron, A.J., and F.D. Patton (1985), The Vaiont Slide, US Corps of Engineers Technical Report, GL-85-8.

Hu, W., R. Huang, M. McSaveney, X. Zhang, L. Yao, and T. Shimamoto (2018), Mineral changes quantify frictional heating during a large low-friction landslide, Geology, 46: 223-226.

Hungr, O. (2007), Dynamics of Rapid Landslides, In: Sassa, K., H. Fukuoka, F. Wang, and G. Wang, Progress in Landslide Science, Springer, Berlin, Heidelberg, 47-57.

Kilgore, B.D., M.L. Blanpied, J.H. Dieterich (1993), Velocity dependent friction of granite over a wide range of conditions, Geophysical Research Letters, 20(10): 903-906.

Leroueil, S. (2001), Natural slopes and cuts: movement and failure mechanisms, Géotechnique, 51(3): 197-243.

Lucas, A., A. Mangeney, and J.P. Ampuero (2014), Frictional velocity-weakening in landslides on Earth and on other planetary bodies, Nature Communications, 5: 3417.

Lupini, J.F., A.E. Skinner, and P.R. Vaughan (1981), The drained residual strength of cohesive soils, Geotechnique, 31(2): 181-213.

L'vov, B. V. (2002), Mechanism and kinetics of thermal decomposition of carbonates, Thermochimica Acta, 386(1): 1–16.

Ma, S., T. Shimamoto, L. Yao, T. Togo, and H. Kitajima (2014), A rotary-shear low to high-velocity friction apparatus in Beijing to study rock friction at plate to seismic slip rates, Earthquake Science, 27: 469–497.

Marone, C., C.B. Raleigh and C.H. Scholz (1990), Frictional behavior and constitutive modeling of simulated fault gouge, J. Geophys. Res., 95: 7007—7025.

Miao, H., G. Wang, K. Yin, T. Kamai, and Y. Li (2014), Mechanism of the slow-moving landslides in Jurassic red-strata in the Three Gorges Reservoir, China, Engineering Geology, 171: 59-69.

Sassa, K. (1985), The mechanism of debris flows, In: Proceedings of XI International Conference on Soil Mechanics and Foundation Engineering, San Francisco, 3: 1173-1176.

Sassa, K., H. Fukuoka, F.W. Wang, and G. Wang (2005), Dynamic properties of earthquake-induced large-scale rapid landslides within past landslide masses, Landslides, 2(2): 125-134.

Sassa. K., H. Fukuoka, G.H. Wang, and N. Ishikawa (2004), Undrained dynamic-loading ring-shear apparatus and its application to landslide dynamics, Landslides, 1: 7-19.

Saito, R., H. Fukuoka, K. Sassa (2006), Experimental study on the rate effect on the shear strength, In: Disaster Mitigation of Debris Flows, Slope Failures and Landslides, Tokyo, Japan, 421-427.

Scaringi, G., C. Di Maio (2016), Influence of displacement rate on residual shear strength of clays, Procedia Earth and Planetary Science, 16: 137-145.

Scaringi, G., W. Hu, Q. Xu, and R. Huang (2017), Shear-rate-dependent behavior of clayey biomaterial interfaces at landslide stress levels, Geophysical Research Letters, 45(2), 766-777.

Segall, P., A.M. Rubin, A.M. Bradley, and R.R. James (2010), Dilatant strengthening as a mechanism for slow slip events, Journal of geophysical research, 115: B12305.

Shimamoto, T., and A. Tsutsumi (1994), A new rotary-shear high-speed frictional testing machine: its basic design and scope of research, Journal of Structural Geology, 39, 65-78.

Singh, A., D. Sitaram, M. Kamruddish, P.K. Ajikumar, A.K. Tyagi, V.S. Raghunathan, and B. Raj (2002), Formation of nanocrystalline calcia by the decomposition of calcite, Journal of the American Ceramic Society, 85(4): 927—932.

Song, Y., D. Huang, and D. Cen (2016), Numerical modelling of the 2008 Wenchuan earthquake-triggered Daguangbao landslide using a velocity and displacement dependent friction law, Engineering Geology, 215: 50-68.

Tika, T.E., P.R. Vaughan, and L. Lemos (1996), Fast shearing of pre-existing shear zones in soil, Geotechnique, 46: 197-233.

Voight, B., and C. Faust (1982), Frictional heat and strength loss in some rapid landslides, Géotechnique, 32: 43-54.

Wang, F.W. and K. Sassa (2000), Relationship between grain crushing and excess pore pressure generation by sandy soils in ring shear tests, Journal of Natural Disaster Science, 22(2), 87-96.

Wang, G., A. Suemine, and W.H. Schulz (2010), Shear-rate-dependent strength control on the dynamics of rainfall-triggered landslides, Tokushima Prefecture, Japan, Earth Surface and Process Landforms, 35: 407-416.

Wu, L.Z., H. Deng, R.Q. Huang, L.M. Zhang, X.G. Guo, and Y. Zhou (2019) Evolution of lakes created by landslide dams and the role of dam erosion: A case study of the Jiajun landslide on the Dadu River, China, Quaternary International, 503A: 41–50.

Wu, L.Z., Y. Zhou, P. Sun, J.S. Shi, G.G. Liu, and L.Y. Bai (2017), Laboratory characterization of rainfall-induced loess slope failure, Catena, 150: 1–8.

Xu, Q., X. Fan, R. Huang, Y. Yin, S. Hou, X. Dong, M. Tang (2010), A catastrophic rockslide debris flow in Wulong, Chongqing, China in 2009: background, characterization, and causes, Landslides, 7: 75-87.

Yao, L., S. Ma, A.R. Niemeijer, T. Shimamoto, J.D. Platt (2016), Is frictional heating needed to cause dramatic weakening of nanoparticle gouge during seismic slip? Insights from friction experiments with variable thermal evolutions, Geophysical Research Letters, 43, 6852-6860.

Yang, C., W. Yu, J. Dong, C. Kuo, T. Shimamoto, and C. Lee (2014), Initiation, movement, and run-out of the giant Tsaoling landslide- What can we learn from a simple rigid block model and a velocity-displacement dependent friction law? Engineering Geology, 182: 158-181.

Yin, Y., P. Sun, M. Zhang, and B. Li (2011), Mechanism on apparent dip sliding of oblique inclined bedding rockslide at Jiweishan, Chongqing, China, Landslides, 8(1): 49-65.

Zhang, M., and M. McSaveney (2018), Is air pollution causing landslides in China? Earth and Planetary Science Letters, 481: 284-289.

Zhang, M., M. McSaveney, H. Shao, and C. Zhang (2018), The 2009 Jiweishan rock avalanche, Wulong, China: Precursor conditions and factors leading to failure, Engineering Geology, 233: 225-230.

Zhang, M., and Y. Yin (2013), Dynamics, mobility-controlling factors and transport mechanisms of rapid long-runout rock avalanches in China, Engineering Geology, 167: 37-58.

Zhang, M., Y. Yin, and M. McSaveney (2016), Dynamics of the 2008 earthquake-triggered Wenjiagou Creek rock avalanche, Qingping, Sichuan, China, Engineering Geology, 200: 75-87.

Zhang, M., Y. Yin, R. Hu, S. Wu, and Y. Zhang (2011), Ring shear test for transform mechanisms of slide-debris flow, Engineering Geology, 118, 55-62.